Ab Initio Modeled Matrix Trapping Sites, PES Asymmetry, and Automerization in the Ar/Cyclobutadiene System†

Richard L. Redington

Department of Chemistry and Biochemistry, Texas Tech University, Lubbock, Texas 79409

Received: November 12, 1999

The symmetrical geometries of 1,3-cyclobutadiene (CB) and substitutional vacancies in crystalline fcc Ar allow purely ab initio MO estimations to be made for the stabilization energies of several symmetric trapping sites in the Ar/CB matrix system at the MP2/6-311++G(2d,2p) [denoted HI-MO] level of theory. The single-substitutional vacancy supports the most stable trapping site in the HI-MO Ar/CB system. It was examined by filling an Ar_{13} vacancy of the HI-MO Ar lattice with a symmetrical CB:Ar_{12} kernel cluster, with dilation of the kernel cluster opposed by a symmetrical HI-MO lattice distortion PEF derived for the purpose. In addition, various supplemental HI-MO stabilization energies were computed. Slightly displacing the four nearest-neighbor Ar atoms coplanar with CB from square-planar geometry shows this site distortion PEF is very soft. The results suggest fluxional behavior for the Ar atoms near the CB guest molecule and the soft trapping site environment provides access to equivalent global PES minima for the two valence isomers of CB. The fast automerization coordinate of CB acts in the presence of slow lattice coordinates to account for the unique spectroscopic observations on Ar/CB reported from the laboratories of J. Michl. These show (a) that CB automerizes at a rate $\geq 10^3$ s^{-1} in cold matrices; (b) that equal populations exist for the matrix-isolated vicinally dilabeled (^{13}C or D) CB valence isomers; and (c) that the automerization ZP energy levels of matrix-isolated CB are separated by an amount $\Delta \geq 35$ cm^{-1}. Trapping sites for CB based on multiple Ar vacancies are not only computed to be less stable than the SS site, but they are unable to support a satisfactory explanation for the experimental observations.

1. Introduction

Pseudo-Jahn−Teller distortion induces rectangular geometry for the 1,3-cyclobutadiene (CB) molecule in its ground electronic state, and the two interconvertable valence isomers give this experimentally difficult molecule potential importance to the field of intramolecular tunneling dynamics. Carpenter[1] was the first to propose that quantum tunneling may be a significant contributor to the rate of valence isomerization (automerization) by CB. His research stimulated experimental[2−4] and theoretical[5−10] work aimed at characterizing the process and recent results[11] identified nonautomerizing, as well as automerizing, vibrational state-specific and isotopomer-specific anharmonic spectroscopic behavior. The zero-point energy level splitting for gaseous $^{12}C_4H_4$ was estimated to be near 11 cm^{-1} to suggest a ZP tunneling rate verging on the picosecond time scale. The analysis combined (a) the vibrational spectra of low-temperature matrix-isolated CB isotopomers obtained by Arnold and Michl;[3] (b) the twenty configuration MCSCF/6-31G MO computation of the square-planar CB saddle-point by Nakamura et al.;[7] (c) MO-computed vibrational spectra for CB isotopomers at the MP2/6-311++G(2d,2p) level [here called HI-MO]; and (d) computed 1-D PES profiles for $^{12}C_4H_4$ along automerization coordinates originating as the C═C stretching normal mode. The analysis smoothly melded the patently nonharmonic Raman transitions observed at 723 and 1678 cm^{-1} for Ar/CB matrix samples with the low MO-computed[7] value of 3.2 kcal/mol (1119 cm^{-1}) for the ZPE-corrected saddle-point energy of D_{4h} CB.

Michl and his collaborators[2−4] studied seven CB isotopomers isolated in Ar and Ne matrices using IR, Raman, and ^{13}C-NMR spectroscopies. No spectroscopic tunneling doublets were observed; however, IR polarization measurements[3] and ^{13}C-NMR line shape analysis[2] of vicinally ^{13}C-dilabeled CB isolated in Ar suggested an automerization rate $\geq 10^3$ s^{-1}, i.e., a rate for these matrix-isolated isotopomers that is fast on the time scale of the NMR experiments. Computations by Carsky and Michl[10] for the vibrational state-specific tunneling splittings of the three lowest-frequency vibrations with a_g symmetry species were based on an MO-computed PES with an automerization barrier of about 10 kcal/mol, and on this basis the tunneling splitting for the automerization fundamental of gaseous $^{12}C_4H_4$ was estimated to be 70 cm^{-1}. Carsky and Michl[10] addressed the failure to observe spectroscopic tunneling structure[4] for CB isolated in Ar or Ne by suggesting that CB and its matrix trapping site are unlikely to have the same symmetry properties. They stated[10] that at the S/N of the Raman experiments a ZP energy level separation $\geq$ 100 cal/mol (i.e. ≥ 35 cm^{-1}) between nonequivalent valence isomers would preclude the detection of transitions from the thermally depopulated higher energy isomer.

Low temperature rare gas (Rg) matrix solids are useful systems for modeling intermolecular guest−host interactions, and the geometries of CB and the Rg crystals are unusually apt for such work. Until recently it has not been feasible to consider ab initio approaches to the matrix trapping site problem, but the Ar/CB system is addressed here using a moderately high level of ab initio quantum theoretical approximation. MO study of the complex Ar/CB system has obvious limitations, but valuable results are produced due to the inherent symmetry of

† Part of the special issue "Marilyn Jacox Festschrift".

10.1021/jp9940102 CCC: $19.00
Published on Web 03/18/2000

this sample system. Most importantly, the HI-MO predictions for Ar/CB can be directly compared with observations[2−4] on well-annealed experimental samples.

Ab initio approaches to the matrix isolation trapping site problem are important because they intrinsically include the near-neighbor multibody interactions, and because they provide prototypes for the study of more general solvation problems. The feasibility of the ab initio MO approach is addressed here by considering relatively large CB:Ar_n and Ar_n clusters at the nontrivial HI-MO level, followed by the introduction of an ab initio based PEF for symmetrical distortion of the lattice around the matrix trapping sites. Specific objectives include (a) determination of the most probable trapping site for CB in solid Ar; (b) estimations for the magnitudes of the Ar-induced energy offsets between nonequivalently trapped valence isomers of CB in the Ar/CB matrix system; and (c) demonstration that equivalent single-substitutional (SS) trapping sites accommodating the two CB valence isomers exist in the Ar matrix system through fluxional behavior by Ar atoms near the CB guest. Cooperative multidimensional coupling between the CB automerization coordinate and Ar lattice modes can lead, in principle, to potentially observable spectroscopic structure of use for evaluating details of the PES topography and global dynamics of the Ar/CB system.

2. MO Computational Procedures and Introductory Results

The wave functions for 1,3-cyclobutadiene should be expressed as linear combinations of Slater determinants; however, the ground state wave function of the rectangular conformation is dominated by a single[5,7] term and only one determinant was used in all of the present computations. It is essential to include an estimate for the electron correlation energy in the MO computations, and in the present work the second-order Møller−Plesset (MP2) perturbation approach was necessarily used. The highest locally feasible ab initio theoretical level, MP2/6-311++G(2d,2p) [abbreviated HI-MO in this article], is able to reasonably approximate the features of van der Waals contact interactions, and it produces results that are far superior to those obtained at the MP2/6-31G(d,p) [here LO-MO] level of theory. HI-MO vibrational spectra[11] computed for seven isotopomers of CB were shown to correlate well with the observed IR/Raman transitions of Ar/CB, except for a specific set of vibrations showing pronounced anharmonic perturbations associated with the double-well PES of CB. As has already been noted,[11] supporting evidence for the success of computations at a level equivalent to HI-MO is provided by recent computational−experimental research on fluorooxirane,[12,13] a strained ring molecule with a single deep PES minimum. The present computational work includes both full and specifically constrained geometry optimizations on the CB:Ar_n and Ar_n clusters chosen for study, along with numerous single point energy computations. The conclusions depend on energy differences tending to cancel some of the errors inherent in finite level MO computations. All results were obtained using the *Gaussian 94* codes[14] run on DEC AlphaStation 200 4/233 and DEC 433au workstations.

2A. Ar_n Clusters and "HI-MO" Argon. Ab initio quantum-mechanical computations including electron correlation energy estimates can contribute significantly to the characterization of potential energy surfaces for weakly bonded systems. In the present section the stabilization energies of the Ar_2, Ar_3 (D_{3h}), Ar_4 (T_d), Ar_{12}(O_h), Ar_{13} (O_h), and Ar_{20} (D_{2h}) clusters are addressed to examine the general performance of the MP2/6-311++G(2d,2p) [HI-MO] theoretical level, and to establish properties for the host HI-MO Ar lattice into which the HI-MO CB impurity is introduced. Formation energies ΔE_f(cluster) for the clusters were computed from reactions $n\text{Ar} \rightarrow \text{Ar}_n$, and the average energies per Ar atom are plotted as a function of the nearest-neighbor (nn) distance parameter, r_0, in Figure 1A. The energies and r_0 values at the minima are shown in the figure. For the $Ar_{2,3,4}$ clusters r_o is the only distance parameter, and the average Ar−Ar bond PEFs for these clusters are plotted as a function of r_o in Figure 1B. The well of the PEF for HI-MO Ar_2 is wider and shallower than that for the benchmark Ar−Ar pair potential function of Aziz,[15] which has the distance and energy parameters $R_{min} = 3.7570$ Å and $e/k = 143.235$ K (285

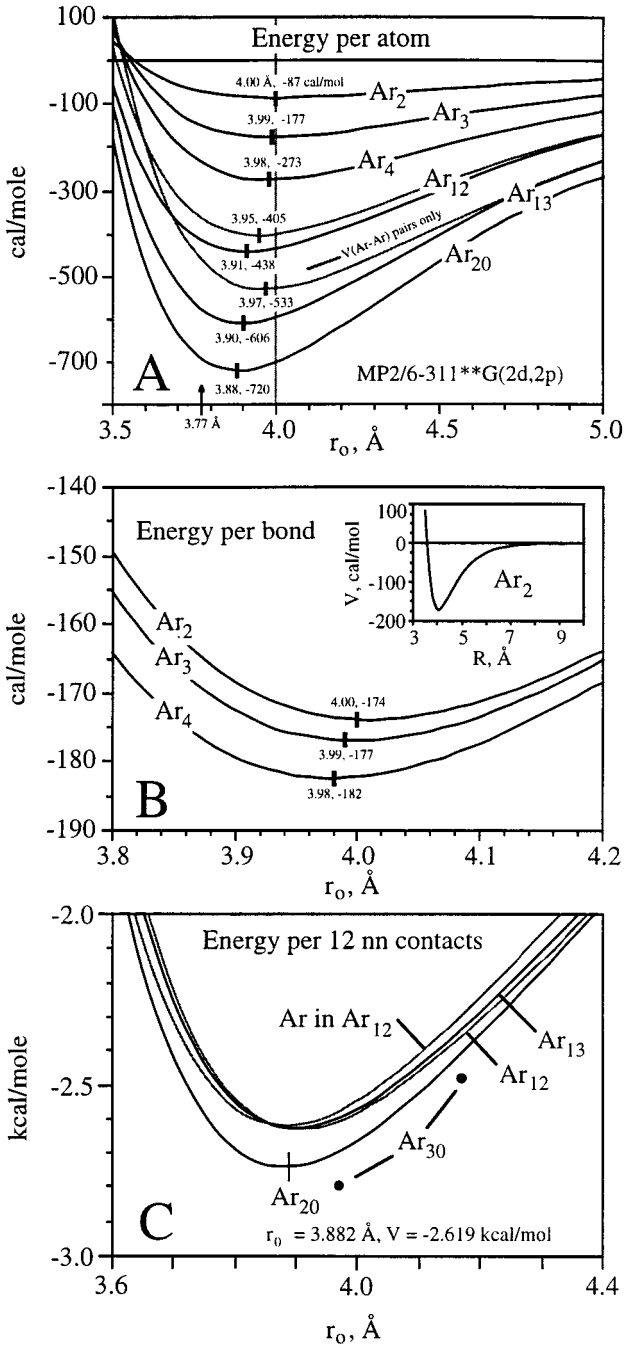

Figure 1. (A) HI-MO energies of formation $\Delta E_f(\text{Ar}_n)$ per atom for symmetrical Ar_n clusters. (B) HI-MO $\Delta E_f(\text{Ar}_n)$ values per bond for Ar_2, Ar_3 (D_{3h}), and Ar_4 (T_d). (C) HI-MO $\Delta E_f(\text{Ar}_n)$ values normalized to 12 nn contacts. The Ar_{12}, Ar_{13}, Ar_{20}, and Ar_{30} clusters have 24, 36, 63, and 104 nn contacts, respectively.

cal/mol). The parameters for HI-MO Ar_2 are $1.06(R_m)_{Aziz}$ and $0.61(e/k)_{Aziz}$. The HI-MO curves for Ar_2, Ar_3, and Ar_4 in Figure 1B are not superimposable and therefore show that significant nonadditive multibody interactions arise at the HI-MO level of MO theory. At $r_o = 4.00$ Å the Ar−Ar energies of the Ar_3 and Ar_4 clusters are about 1.8% and 4.8% lower than the energy of Ar_2, while comparison values obtained by Lotrich and Szalewicz[16] are 1% for Ar_3 and 7% for the Ar crystal. The two gray curves drawn in Figure 1A were computed for the Ar_{12} and Ar_{13} clusters using only the pairwise PEF of HI-MO Ar_2. These curves demonstrate the increasing importance of multibody interactions in HI-MO clusters of increasing size, and they anticipate the much larger multibody interactions found for the CB:Ar_n clusters.

The energy minimum for HI-MO Ar_{20}, a D_{2h} cluster with the atoms stacked Ar_6:Ar_8:Ar_6 in the fcc (0,0,1) planes as discussed below, occurs at $r_o = 3.88$ Å. This is a decrease of only 0.02 Å from r_0 at the energy minimum for Ar_{13} (and a decrease of 0.09 Å from that for Ar_{13} approximated using only the pairwise PEF of HI-MO Ar_2). The 3.88 Å value is 0.11 Å (2.9%) longer than the r_o value of 3.77 Å observed for crystalline Ar(s). The average stabilization energy for an Ar atom in the HI-MO Ar_{20} cluster is −720 cal/mole. This value is much less than that experienced by an average lattice Ar atom because only 2 atoms in Ar_{20} have the full fcc lattice complement of 12 nearest-neighbors (to say nothing of the lattice complements at longer distances).

The r_0-dependent PEF of a typical lattice Ar atom is an important consideration in this work based on scaling the cluster or lattice geometries as a function of r_0. Approximations to this special PEF are shown in Figure 1C where the ΔE_f(cluster) values for Ar_{12}, Ar_{13}, and Ar_{20} are reduced to energies per 12 nearest-neighbor (nn) contacts, i.e., to $\Delta E_f(Ar_{12})/2$, $\Delta E_f(Ar_{13})/3$, and $\Delta E_f(Ar_{20})/5.25$. The Ar_{20} PEF is the deepest of these and it has a slightly shorter r_0 value than the other clusters due to its fuller complement of interatomic Ar interactions. It is chosen to describe the energy of an Ar atom in a lattice that is symmetrically dilated or contracted by scaling the nearest-neighbor distance r_0. The "Ar in Ar_{12}" PEF in Figure 1C results from subtracting the total energy of the Ar_{12} cluster from the total energy of the Ar_{13} cluster as a function of r_0. The resulting PEF, like that for Ar_{20}, has its minimum at $r_o = 3.88$ Å, but this PEF clearly reflects the lack of non-nn interactions experienced by the reference Ar. Two energy points were obtained for the Ar_{30} cluster with Ar_9:Ar_{12}:Ar_9 stacking in (0,0,1), planes and these are included in Figure 1C as $\Delta E_f(Ar_{30})/[104/12]$.

The HI-MO energies $\Delta E_f(Ar_{12})$ and $\Delta E_f(Ar_{13})$ show that the energy to form a central vacancy in the HI-MO Ar_{13} cluster according to the reaction $Ar_{13} \rightarrow Ar_{12} + Ar$ is +2.619 kcal/mol with $r_o = 3.88$ Å for both clusters.

Energies for adsorption of an Ar atom onto the surface of an Ar crystallite, and for the adsorption of CB onto an Ar crystallite surface, are of interest relative to ranking of the stabilities of trapping sites formed by isomerizations of a CB:Ar_N cluster. The HI-MO energy for adsorption of an Ar atom onto a tetragonal surface of the Ar_{13} cluster with $r_0 = 3.90$ Å [$Ar_{13} + Ar \rightarrow Ar_{13}$:Ar] is −0.92 kcal/mol. The standard counterpoise BSSE computation with separation to Ar_{13} and Ar reduces this value to −0.48 kcal/mol. The −0.92 kcal/mol adsorption energy, retained in this work, is slightly larger than one-third of the HI-MO value of −2.619 kcal/mol obtained by inserting Ar in Ar_{12}, to suggest that the interaction energy is dominated by the four nn Ar−Ar van der Waals contacts. The energy for adsorption of an Ar atom onto a hexagonal (1,1,1) surface of HI-MO Ar_{15}, stacked Ar_3:Ar_{12}, is −0.93 kcal/mol with $r_0 = 3.90$ Å. As shown in the inset of Figure 2B, at minimum energy the adsorbed Ar is 3.16 Å from the Ar_{12} plane, a value that is reduced slightly from the hexagonal lattice plane separation of 3.184 Å. As shown in Figure 2 the energy for adsorption of CB onto a hexagonal (1,1,1) surface of Ar_{15} stacked Ar_5:Ar_{10} is −4.505 kcal/mol with CB at a distance of 3.06 Å and symmetrically bridging two Ar atoms. These lie at opposite ends of an energy valley characterizing the PES of the CB:Ar vdW molecule as seen in the following section.

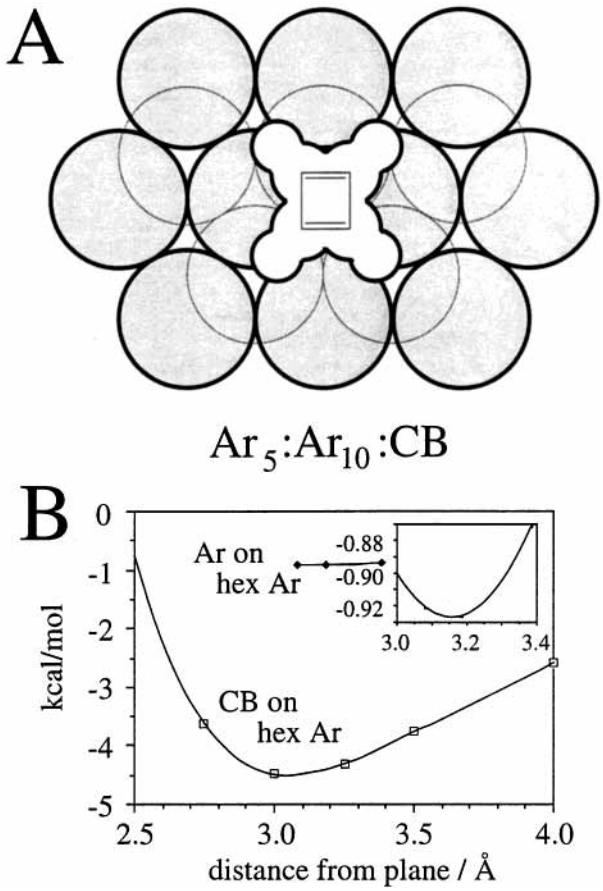

Figure 2. (A) Geometry of the stacked Ar_5:Ar_{10}:CB cluster ($r_0 = 3.90$ Å). The adsorbed CB molecule bridges the central two Ar atoms in the (1,1,1) plane. These atoms are near energy minima found for the HI-MO CB:Ar van der Waals molecule (cf. Figure 3). (B) Dependence of adsorption energy on the separation of CB from the Ar_{10} surface of the Ar_5:Ar_{10} cluster. Inset is for Ar adsorbed on the Ar_{12} surface of Ar_3:Ar_{12}.

2B. The CB:Ar van der Waals Complex. The CB:Ar_n clusters are introduced by describing results obtained at the HI-MO [MP2/6-311++G(2d,2p)] level for the CB:Ar van der Waals molecule. CB:Ar, like all CB:Ar_n clusters, has not been examined by experiment or high level ab initio computation (cf., however, ref 17). Features of the PES topography for CB:Ar are shown through optimized geometries of the complex obtained with Ar successively constrained to each of the symmetry axes of CB. The lowest energy occurs for Ar above the CB plane, but this C_{2v} configuration actually yields a shallow PES saddle point. Minimum energy paths tracked by the Ar atom when it is circled about CB in the vertical symmetry planes are shown in Figure 3A. The path in the plane between the two C═C bonds leads between saddle-point maxima at both $\Theta = 0$ and $\Theta = 90°$.

The stabilization energy for the HI-MO CB:Ar van der Waals

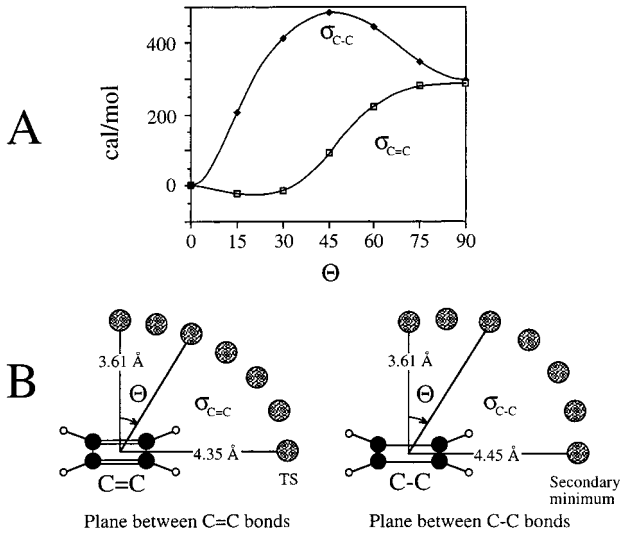

Figure 3. (A) Fully optimized HI-MO energies for CB:Ar along the minimum energy paths for Ar positions in symmetry planes between the C═C bonds and between the C−C bonds. (B) Ar positions along the minimum energy paths shown in part (A).

complex is −0.73 kcal/mol, which decreases to −0.46 kcal/mol[17] with ZPE and counterpoise BSSE corrections (CB and Ar entities) included. This result predicts sufficient stability for CB:Ar that it should be a candidate for future spectroscopic study in cold molecular beam samples. The PES topography outlined in Figure 3 suggests that the vibrationally averaged equilibrium geometry of HI-MO CB:Ar will have no higher than C_s symmetry, and this MO-predicted feature is reminiscent of the offset position for Ar determined in a computational−experimental[18] study of the acetylene:Ar van der Waals molecule. The valence isomers of CB in CB:Ar will have unequal energy minima if CB automerizes suddenly without simultaneous adjustment of the offset Ar position. In contrast, cooperative motion by Ar can access a symmetrically equivalent minimum on the global PES. The multidimensional dynamics of CB:Ar and other CB:X van der Waals molecules present an attractive topic for future spectroscopic and theoretical research. The −4.51 kcal/mol adsorption energy of CB onto the hexagonal plane of Ar_5:Ar_{10} in Figure 2 is more than six times the adsorption energy with a single Ar atom to CB, a result anticipating the major importance of multibody interactions that is seen below for the larger CB:Ar_n clusters.

2C. The Planar CB:Ar_4 Cluster. The CB:Ar_4 cluster with D_{2h} symmetry plays a pedagogical role for the evaluation of the Ar matrix trapping site and for the automerization behavior of matrix-isolated CB. Figure 4 shows CB occupying a single-substitutional (SS) vacancy in the (0,0,1) plane of crystalline Ar (lattice parameter a_o = 5.33 Å; nn distance r_o = 3.77 Å). The octahedral interstitial regions bring the vacancy into near congruence with the geometry of CB, and to emphasize this point the Ar positions determined for the fully optimized HI-MO CB:Ar_4 (D_{2h}) van der Waals configuration (Table 1) are indicated by bold circles. LO-MO vibrational analysis indicates the lack of a strong drive toward nonplanarity by the D_{2h} configuration of CB:Ar_4, as eight of the LO-MO frequency values (four of them imaginary) are less than 1 cm^{-1}. The LO-MO computations yield R_1 and R_2 distances which are 0.19 and 0.18 Å longer, respectively, than the HI-MO values drawn in Figure 4.

As listed in line (b) of Table 2, the energy rises about 1 kcal/mol when R_1 and R_2 of the CB:Ar_4 vdW molecule are compressed halfway to the crystal value of 3.77 Å. Semiempirical

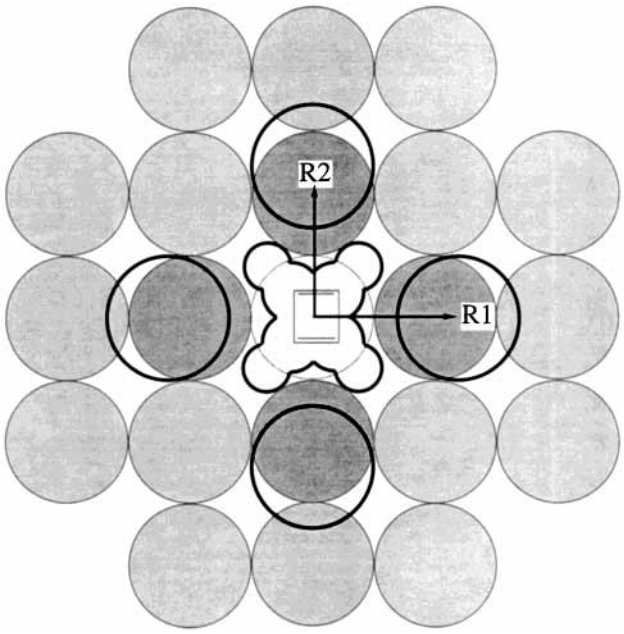

Figure 4. Optimized geometry of the planar CB:Ar_4 van der Waals configuration (bold figures) superposed on a (0,0,1) plane of the fcc Ar crystal lattice. It is seen that if CB automerizes within a frozen Ar_4 vdW configuration it faces an unequal double-minimum PEF. On the other hand, if the pairs of Ar atoms make small shifts to interchange magnitudes of the R_1 and R_2 distances, the system comes to an equivalent minimum in the global PES. The essence of this behavior is substantiated for the single-substitutional Ar matrix trapping site as developed in the text.

TABLE 1: Geometries of CB and the Planar CB:Ar_4 van der Waals Molecule[a]

	basis[b]	$R_{C=C}$	R_{C-C}	R_{CH}	Θ_{C-CH}	R_1	R_2
CB	LO-MO	1.345	1.565	1.079	134.8		
CB	HI-MO	1.344	1.574	1.077	135.1		
CB:Ar_4	LO-MO	1.345	1.566	1.079	134.8	4.524	4.626
CB:Ar_4	HI-MO	1.345	1.573	1.077	135.2	4.335	4.445
CB:Ar_4	HI-MO	1.343	1.566	1.074	134.6	3.77	3.77

[a] D_{2h} symmetry, distances in Å, angles in degrees, R_1 and R_2 defined in Figure 4. [b] LO-MO is MP2/6-31G(d,p), HI-MO is MP2/6-311++G(2d,2p).

TABLE 2: CB:Ar_4 (D_{2h}) Cluster Energies and PES Offsets[a]

	Ar_4 geometry[b]		$E - E_{vdW}$	offset of PES minima	
	R_1	R_2	kcal/mol	Δ, cm^{-1}	
(a) vdW	4.335	4.445	0.0	23.7	optimized
(b) 50% to Xstal	4.052	4.107	0.967	50.2	CB opt.
(c) 75% to Xstal	3.911	3.939	2.916	45.4	CB opt.
(d) crystal	3.77	3.77	6.963	0.0	CB opt.
(e) 50% | vdW	4.052	4.445	0.373	191.1	CB opt.

[a] HI-MO = MP2/6-311++G(2d,2p). [b] The CB:Ar_4 structure appears in Figure 4.

estimates have been made for the displacements of Ar atoms from their normal lattice positions when stressed by the presence of a guest molecule larger than Ar in an Ar crystal vacancy. Such results include research by Gunde et al.[19] on Ar_{366} clusters containing one trans or one gauche difluoroethane molecule, and by Lakhlifi and Girardet[20] on Ar/CH_3F trapping sites. For these systems outward displacements of 0.3−0.4 Å are computed for the closest nn Ar atoms, with smaller displacements arising for Ar atoms located further from the guest molecule. The computations presented below for CB in HI-MO Ar suggest a dilation of 0.19 Å for the 12 nearest-neighbor Ar atoms

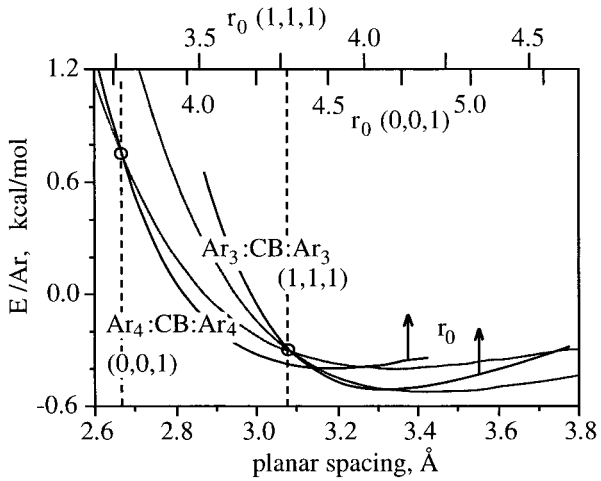

Figure 5. Black lines: the r_0 (upper scale) and layer spacing dependence of HI-MO $\Delta E_{sub}^{(n,m)}$(cluster) for reactions Ar_{n+1} + CB → CB:Ar_n + Ar with stacked Ar_3:CB:Ar_3 (C_{2v}) and stacked Ar_4:CB:Ar_4 (D_{2h}) clusters. Gray lines: layer spacing dependence of $\Delta E_{sub}^{(n,m)}$(cluster) obtained with geometries of the planar Ar_n moieties determined by r_0 = 3.77 Å. Dashed lines connect r_0 = 3.77 Å (upper scales) with layer spacings of the (0,0,1) and (1,1,1) planes (lower scale). The C═C bonds in Ar_3:CB:Ar_3 parallel a leg of the equilateral Ar_3 triangle.

surrounding CB in the symmetrical and nearly congruent single-substitutional matrix trapping site.

The energy offsets Δ arising between PES minima of the valence isomers of CB automerized in CB:Ar_4 with rigid Ar_4 moieties are included in column 5 of Table 2. Lines a−d show Δ values for Ar_4 geometries scaled between the vdW and real lattice limits. These values maximize around 50 cm^{-1}, while line e, with Δ = 191 cm^{-1}, illustrates the much larger Δ value arising from a more pronounced rectangular Ar_4 configuration. More physically meaningful Δ values produced in 3-D CB:Ar_n kernel clusters are found below.

2D. Stacked Ar_n:CB:Ar_n Clusters. Interaction energies between CB and Ar atom layers stacked above and below it and centered on a common symmetry axis are considered in this section, and Figure 5 shows the geometry dependent energies for the reactions Ar_n:Ar:Ar_n + CB → Ar_n:CB:Ar_n + Ar. The gray lines show r_0-dependent energies (expressed per Ar atom) when the planar separations are varied while holding the CB geometry frozen at its free molecule value and with the square Ar_4, and triangular Ar_3, geometries frozen with r_o = 3.77 Å. At the circled reference points the Ar clusters are standard fcc lattice fragments with the planar spacings $r_o\sqrt{(1/2)}$ = 2.666 Å for (0,0,1) planes and $r_o\sqrt{(2/3)}$ = 3.078 Å for (1,1,1) planes. The black curves show the r_0-dependent cluster energies with geometries of the complete Ar_8 and Ar_6 lattice fragments scaled by r_0.

The PEFs in Figure 5 suggest that clusters with CB lying in the (0,0,1) plane may be unstable relative to the neat Ar clusters when r_0 < 4 Å because of the repulsive interactions between the π system of CB and the adjacent stacked Ar atoms. However, HI-MO computation of the full CB:Ar_{12} cluster shows this entity is stable relative to Ar_{13} over a large range of r_o values, again serving to emphasize the important multibody interactions produced in a cluster by the presence of CB, in this case in close contact with 12 nn Ar atoms. The CB:Ar_{12} vdW cluster is used as the kernel of the single-substitutional trapping site with CB lying in a (0,0,1) plane of fcc HI-MO Ar. Double- triple- and quadruple-substitutional sites with CB lying in the (1,1,1) and (0,0,1) planes are considered below using different kernel clusters.

3. CB:Ar_n Kernel Clusters for *m*-Ar Substitutional Trapping Sites in HI-MO Ar/CB

3A. Kernel Cluster Energies. The energies of formation ΔE_f(cluster) for pure Ar or CB-doped Ar clusters are defined for the gas-phase reactions

$$m\mathrm{Ar} + n\mathrm{Ar} \rightarrow \mathrm{Ar}_m{:}\mathrm{Ar}_n \quad (1)$$

$$\mathrm{CB} + n\mathrm{Ar} \rightarrow \mathrm{CB}{:}\mathrm{Ar}_n \quad (2)$$

with

$$\Delta E_f(\mathrm{Ar}_m{:}\mathrm{Ar}_n) = E(\mathrm{Ar}_m{:}\mathrm{Ar}_n) - (m+n)E(\mathrm{Ar}) \quad (3)$$

$$\Delta E_f(\mathrm{CB}{:}\mathrm{Ar}_n) = E(\mathrm{CB}{:}\mathrm{Ar}_n) - nE(\mathrm{Ar}) - E(\mathrm{CB}) \quad (4)$$

The energies for gaseous reactions substituting CB for m Ar atoms within an Ar_m:Ar_n cluster,

$$\mathrm{Ar}_m{:}\mathrm{Ar}_n + \mathrm{CB} \rightarrow \mathrm{CB}{:}\mathrm{Ar}_n + m\mathrm{Ar} \quad (5)$$

are denoted $\Delta E_{sub}^{(n,m)}$, e.g.

$$\Delta E_{sub}^{(n,m)}(\mathrm{CB}{:}\mathrm{Ar}_n) = E(\mathrm{CB}{:}\mathrm{Ar}_n) + mE(\mathrm{Ar}) - E(\mathrm{Ar}_m{:}\mathrm{Ar}_n) - E(\mathrm{CB})$$

$$= \Delta E_f(\mathrm{CB}{:}\mathrm{Ar}_n) - \Delta E_f(\mathrm{Ar}_m{:}\mathrm{Ar}_n) \quad (6)$$

The r_o-dependent curves for HI-MO ΔE_f(Ar:Ar_{12}), ΔE_f(CB:Ar_{12}), and $\Delta E_{sub}^{(12,1)}$ (CB:Ar_{12}) are shown in Figure 6A, where a −5.70 kcal/mol stabilization of [CB:Ar_{12} + Ar] relative to [Ar_{13} + CB] is seen to occur at r_o = 4.43 Å for the gaseous species. This stabilization energy is significantly larger than might be construed from computations for smaller clusters. For example, multiplying the −0.40 (kcal/mol)/atom stabilization energy of the stacked Ar_4:CB:Ar_4 cluster in Figure 5 by 12 as an estimate for the energy of CB:Ar_{12} yields only −4.80 kcal/mol. The HI-MO data points producing the curves in Figure 6A are listed in Table 3.

The r_0-dependent $\Delta E_{sub}^{(n,m)}$ (CB:Ar_n) energies cannot describe matrix trapping sites because the cluster dilates to its minimum energy configuration free of constraint from the bulk Ar lattice, and a function for estimating the HI-MO lattice distortion energy is introduced in the following section.

3B. The HI-MO V_{latt} Function. Basic intuition, backed by the results of published trapping site research such as the studies of refs 19 and 20, suggests that displacements of lattice Ar atoms from their equilibrium neat lattice positions generally decrease as their distance from an introduced defect site is increased. The nn distance r_o and the lattice parameter a_o of the fcc lattice are related as $a_o = \sqrt{2}r_o$, and the radial distances of lattice points to a reference lattice point chosen as the origin are given by the radii r_n of hypothetical spheres: $r_1 = \sqrt{1}r_o$ (12 Ar on the sphere), $r_2 = \sqrt{2}r_o$ (6 Ar), $r_3 = \sqrt{3}r_o$ (24 Ar), ..., $r_n = \sqrt{N}r_o$ (where N is a specifically calculated number of Ar atoms lying on the nth sphere, e.g., for r_{49} and r_{50} the values of N are 108 and 30, respectively).

Two limiting forms for a symmetric lattice distortion function, V_{latt}, are obtained by supposing that the guest molecule symmetrically dilates the first sphere of atoms surrounding a single-substitutional site (12 Ar atoms at radius $r_1 = \sqrt{1}r_o$) to generate a dilation volume $\Delta V = 4\pi r_1^2 \Delta r_1$. As the first limit, it is assumed that the n_2 and higher shells are unaffected by the r_1 dilation and remain undilated; as the second limit it is assumed that the first shell dilation volume ΔV is preserved in the r_2

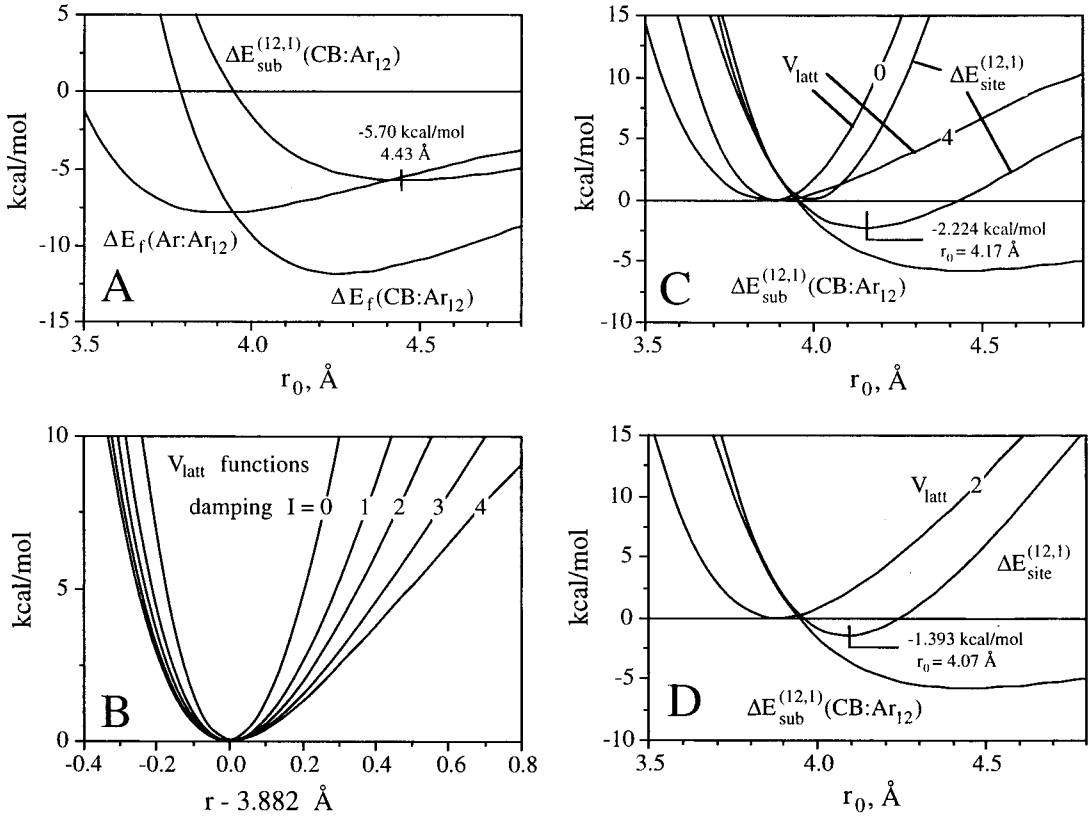

Figure 6. (A) The $\Delta E_f(Ar:Ar_{12})$, $\Delta E_f(CB:Ar_{12})$, and $\Delta E_{sub}^{(12,1)}(CB:Ar_{12}) = \Delta E_f(Ar:Ar_{12}) - \Delta E_f(CB:Ar_{12})$ curves. Data points are in Table 3. (B) Radial lattice distortion PEFs V_{latt}. Curve ($I = 0$) preserves the r_1 shell displacement volume ΔV for all shells; curve ($I = 4$) has ΔV damped to zero for all shells r_n beyond r_1; curve ($I = 2$) is the intermediate damped V_{latt} function used for the trapping site computations. The origin is at $r_0 = 3.882$ Å for HI-MO Ar. (C) $\Delta E_{site}^{(12,1)} = \Delta E_{sub}^{(12,1)}(CB:Ar_{12}) + V_{latt}^{(I)}$ curves for $I = 0$ (undamped) and $I = 4$ (fully damped). (D) $\Delta E_{site}^{(12,1)} = \Delta E_{sub}^{(12,1)}(CB:Ar_{12}) + V_{latt}^{(2)}$ curve with I = 2 used for the single-substitutional trapping site.

TABLE 3: HI-MO Energies for Single-Substitutional Site in Ar/CB (CB in (0,0,1) plane)[a]

r_0	$\Delta E_f(Ar:Ar_{12})$	$\Delta E_f(CB:Ar_{12})$	$\Delta E_{sub}^{(12,1)}$	V_{latt}[b]	$\Delta E_{site}^{(12,1)}$[c]
3.37	6.7220			37.9354	
3.57	−3.9954			10.2660	
3.77	−7.4455	1.1964	8.6419	0.9627	8.6419
3.87	−7.8563	−4.8571	2.9992	0.0095	3.0087
3.97	−7.8081	−8.6791	−0.8710	0.4388	−0.4322
4.07	−7.4879	−10.6218	−3.1339	1.7415	−1.3924
4.17	−7.0187	−11.5888	−4.5701	3.5943	−0.9758
4.37	−5.9179	−11.6055	−5.6876	8.3015	2.6139
4.57	−4.8356	−10.4325	−5.5969	13.8913	8.2944
4.77	−3.8827	−8.9228	−5.0401	19.6396	14.5995

[a] $CB:Ar_{12}$ kernel cluster appears in Figure 7A. ΔE energy definitions are in eqs 3, 4, 6, and 13. r_0 is Å and energies are kcal/mol. [b] Equation 9. Lead "12" in eq 11 is adapted to 12(7/12) = 7; see text. [c] Stabilization energy contribution: −1.39 kcal/mol at $r_0 = 4.07$ Å.

shell and in all higher shells. The displacements of the spherical shells at r_2, r_3, ... r_n are then given as $\Delta V = 4\pi r_1^2 \Delta r_1 = 4\pi r_n^2 \Delta r_n$ for all values of n, and with $\Delta r_n = (r_1/r_n)^2 \Delta r_1 = (1/n)\Delta r_1$ it is seen that Δr_n approaches zero for large values of n. The lattice distortion energy generated for this V_{latt} model is estimated by summing the radial distortion energies of all atoms on all spheres under the assumption that the same 1-D radial displacement PEF, designated $u(\Delta r_n)$, is valid for each atom. Thus, with the summation truncated at the kth sphere,

$$V_{latt} = 12u(\Delta r_1) + 6u(\Delta r_2) + 24u(\Delta r_3) + 12u(\Delta r_4) + ... + N_k u(\Delta r_k) \quad (7)$$

This energy summation is readily expressed when $u(\Delta r)$ is written as a polynomial in Δr, e.g.,

$$u(\Delta r) = k\Delta r^2 + a\Delta r^3 + b\Delta r^4 + c\Delta r^5 \quad (8)$$

Substituting the $u(\Delta r)$ polynomial into eq 7 for V_{latt} yields

$$V_{latt} = Kk\Delta r_1^{\,2} + Aa\Delta r_1^{\,3} + Bb\Delta r_1^{\,4} + Cc\Delta r_1^{\,5} \quad (9)$$

where the constant K is defined as the expansion

$$K = [\,12(r_1/r_1)^\alpha + 6(r_1/r_2)^\alpha + 24(r_1/r_3)^\alpha + 12(r_1/r_4)^\alpha + ... + N_k(r_1/r_k)^\alpha\,] \quad (10)$$

$$= [12 + 6(1/2)^\alpha + 24(1/3)^\alpha + 12(1/4)^\alpha + ... + N_k(1/k)^\alpha] \quad (11)$$

with $\alpha = 2$. Equation 11 defines the constants A, B, and C by using $\alpha = 3$ for A, 4 for B, and 5 for C. For the fcc lattice, the constants K, A, B, and C converge to values of 25.224, 14.4539, 12.8019, and 12.3113, respectively, where, as seen in eq 11, the r_1 shell contributes the value 12 to each of these numbers. The constant K converges much more slowly than the constants A, B, and C as a function of n, and the estimate $K = 25.224$ is an extrapolation to the infinite crystal limit of the sum 25.0138 obtained by direct summation of all shells to r_{6000}. The summation increments closely follow an exponential function for the shells beyond r_{4000}. With ΔV conserved, this V_{latt} function might affect 10^6 lattice atoms, since the r_{4000} radius is 63.2 r_o = 247 Å for $r_0 = 3.90$ Å. The derivative dr/dn at r_{4000} is 0.031 Å, a value entering the range of thermal vibrational amplitudes for the low temperature Ar crystal. Involving the displacement

TABLE 4: V_{latt} Coefficients K,[a] A, B, and C

index I	$D(I)$[b]	K ($\alpha = 2$)	A ($\alpha = 3$)	B ($\alpha = 4$)	C ($\alpha = 5$)
0	$n^{-0.00}$	25.224	14.45385	12.80194	12.31125
1	$n^{-0.25}$	16.9646	13.03776	12.31125	12.10740
2	$n^{-0.50}$	14.45387	12.49255	12.13188	12.04002
3	$n^{-1.00}$	12.80194	12.13188	12.02736	12.00628
4	$n^{-\infty}$	12.00000	12.00000	12.00000	12.00000

[a] Equation 11. [b] Damping factors for ΔV. See section 3B.

of so many Ar atoms, this version of the V_{latt} function is quite stiff and factors were introduced to damp the Δr_n displacements and soften the PEF. Damping factors $D^{(0)} = 1.0$ [no damping], $D^{(1)} = n^{-0.25}$, $D^{(2)} = n^{-0.50}$, $D^{(3)} = n^{-1.0}$, and for $n > 1$ $D^{(4)} = n^{-\infty}$, were entered into the Δr_n equations for shell displacements to yield $\Delta r_n = (1/n)D^{(I)}\Delta r_1$ for $I = 0$ to 4. The coefficients $K^{(I)}$, $A^{(I)}$, $B^{(I)}$, and $C^{(I)}$ are listed in Table 4.

The PEF curve for Ar_{20} shown in Figure 1C (cf. section 2) was selected for use as $u(\Delta r)$; a PEF intended to approximate the energy of an Ar lattice atom subjected to dilation or contraction of the surrounding fcc lattice of HI-MO Ar. Eight equally spaced HI-MO PEF points along the $u(\Delta r) = \Delta E_f(Ar_{20})/5.25$ curve were evaluated between $r_o = 3.37$ to 4.77 Å to determine the constants k, a, b, and c in eq 8. The points were fitted to a fifth-order polynomial with the origin placed at the PEF minimum as a part of the least-squares fitting process. The resulting equation for $u(\Delta r)$ is

$$u(\Delta r) = 6.5000\Delta r^2 - 11.9997\Delta r^3 + 11.9517\Delta r^4 - 5.0075\Delta r^5 \quad (12)$$

where the units are kcal/mol for $u(\Delta r)$ and Å for Δr. The kK, aA, bB, and cC parameters for $V_{latt}^{(I)}$ are then obtained using Table 4. At the minimum energy value for $u(\Delta r)$ r_o is 3.882 Å, and this value is used for r_o of the undistorted HI-MO Ar lattice. The five $V_{latt}^{(I)}$ curves are plotted in Figure 6B, where the effect of progressively damping the higher shell Δr displacements is seen to soften the PEF. The intermediate curve, $V_{latt}^{(2)}$, is chosen as V_{latt} for the Ar/CB trapping site computations.

3C. The Single-Substitutional Ar Matrix Trapping Site of CB. When it is constrained by V_{latt} the $\Delta E_{sub}^{(n,m)}(CB{:}Ar_n)$ function (eqs 5 and 6) for the van der Waals kernel cluster provides first input to the stabilization energy of an m-Ar substitutional matrix trapping site. The combined functions for the SS site,

$$\Delta E_{site}^{(12,1)} = \Delta E_{sub}^{(12,1)}(CB{:}Ar_{12}) + V_{latt}^{(I)} \quad (13)$$

based on the limiting $I = 0$ and $I = 4$ forms of V_{latt} are plotted in Figure 6C. The $\Delta E_{site}^{(12,1)}$ PEF based on the undamped V_{latt} ($I = 0$) shows no site stabilization energy because the stiffness of this V_{latt} function prevents access to the region of large r_0 where the kernel cluster is well stabilized. At the limit of fully damped V_{latt} with $I = 4$, the $\Delta E_{site}^{(12,1)}$ PEF has a stabilization energy of -2.22 kcal/mol at $r_0 = 4.17$ Å, corresponding to an r_1 dilation of $4.17 - 3.88 = 0.29$ Å. Figure 6D shows the $\Delta E_{site}^{(12,1)}$ curve obtained using the intermediate ($I = 2$) V_{latt} function chosen as the lattice distortion PEF. The $\Delta E_{site}^{(12,1)}$ contribution to the SS site stabilization energy is -1.39 kcal/mol at $r_0 = 4.07$ Å, i.e., with an r_1 dilation of 0.19 Å. The -1.39 kcal/mol value is a lower limit to the SS site stabilization energy, which is tripled by including two necessary additional stabilization energies presented below. The $\Delta E_{site}^{(12,1)}$ values are points from Table 3.

Before its summation to $\Delta E_{sub}^{(12,1)}(CB{:}Ar_{12})$ the V_{latt} function must be adapted to the SS vacancy by reducing the atom count from 12 to 7 in the n_1 shell of eq 11 for K, A, B, and C. There are 12 nn contacts for each Ar of the n_1 shell in V_{latt}, and 5 nn contacts for these same Ar atoms in $\Delta E_{sub}^{(12,1)}(CB{:}Ar_{12})$ when CB−Ar contacts are counted as equivalent to Ar−Ar contacts. Weighting each of the n_1 shell Ar atoms in V_{latt} by the factor 7/12 produces 12 nn contacts distributed over the two functions. For sites based on m-Ar vacancies, the V_{latt}-lattice interface is treated by replacing the leading 12 in K, A, B, and C by $(7/12)X$, where X is the number of Ar atoms deemed to make nn contact with CB. The use of larger kernel clusters would obviate these procedures since the shared Ar atoms at the kernel-lattice interface layer at the n_5 shell, for example, would be surrounded by 12 Ar atoms approximating a more nearly lattice-like environment than at r_1. Moreover, Δr_5, not Δr_1, would provide the leading displacement for $V_{latt.}$ Absorbing the most geometry-sensitive energies directly into the HI-MO $\Delta E_{sub}^{(n,m)}(CB{:}Ar_n)$ computation greatly reduces and simplifies the role of V_{latt}.

An important kernel-lattice interface energy correction was found that significantly increases the stabilization of the SS site based on the $CB{:}Ar_{12}$ kernel by comparing the energies for adsorbing Ar onto the faces of $CB{:}Ar_{12}$ versus Ar_{13} clusters. The energy correction in question is unique to the SS site and would be automatically included in $\Delta E_{sub}^{(18,1)}(CB{:}Ar_{18})$ and larger kernel cluster computations carrying the n_2 shell Ar atoms. For now, using $r_o = 3.90$ Å for the Ar_{12} and Ar_{13} lattice fragments, the energies are -0.92 kcal/mol for adsorption of an Ar onto the Ar_{13} surfaces, versus -1.42 kcal/mol for its adsorption onto one of the four surfaces placing it coplanar with CB in $CB{:}Ar_{12}$, and -1.06 kcal/mol for its adsorption onto one of the surfaces placing it above or below the plane of CB. In the trapping site context this result suggests that at least -2.26 kcal/mol of extra stabilization energy is added to the SS site. The energy is due to interactions involving CB with the 6 Ar atoms in the $n = 2$ (second nn) shell. This energy of the r_2 shell is absent in the V_{latt} function based on pure Ar. Judging from the trapping site geometry in Figure 7A, the extra stabilization energy arises through interactions involving polarization of the four Ar atoms mildly impinged by CH bonds, and it is most likely the strongest stabilizing interaction involving atoms outside the $CB{:}Ar_{12}$ van der Waals kernel cluster. This energy is included in column 6 of Table 5 reserved for "special", aka "stabilization energy unique to this kernel" entries.

The $\Delta E_{site}^{(n,m)}$ PEFs are zeroed relative to gaseous CB and m gaseous Ar atoms in the defining chemical equations. The Ar/CB trapping site energies are more realistically described when the m gaseous Ar atoms appearing in eq 6 are adsorbed onto outer surfaces of the CB-doped crystallite and these energies, -0.93 kcal/mol per adsorbed Ar atom, are entered into column 5 of Table 5. In section 2A the stabilization energy obtained by the adsorption of CB onto a hexagonal Ar surface was approximated as -4.51 kcal/mol by using the Ar_{15} cluster. This stabilization energy ranks external surface adsorption as a major competitor of the internal trapping sites and it is entered with them in Table 5. The stabilization energies entered into Table 5 narrowly rank the single-substitutional trapping site as the most stable site in HI-MO Ar/CB.

3D. PES Asymmetry in the SS Site and the Automerization Mechanism in Ar/CB. Distorting the highly symmetrical SS vacancy to more nearly match the nonspherical geometry of CB adds to the SS site stabilization, and first steps taken to investigate effects of the asymmetry are now described. The four nearest neighbor Ar atoms coplanar with CB were offset

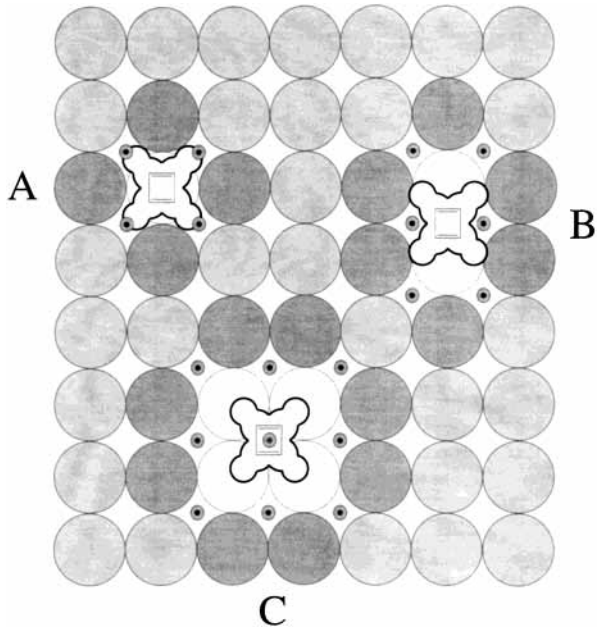

Figure 7. Definitions for CB:Ar$_n$ kernel clusters and *m*-Ar vacancies with CB lying in the (0,0,1) plane of fcc Ar. (A) SS site, CB:Ar$_{12}$ kernel. (B) DS site, CB:Ar$_{18}$ kernel. (C) QS site, CB:Ar$_{26}$ kernel. Together with CB the darker shaded Ar atoms indicate the CB:Ar$_n$ kernel clusters. The small circles and heavy dots represent positions of Ar atoms in the planes above and below the plane of CB.

TABLE 5: Summary of Trapping Site Stabilization Energies (kcal/mol) for the HI-MO Ar/CB Matrix System

CB site	host plane	figure	$\Delta E_{sub}^{(n,m)} + V_{latt}$[a]	surface	special[b]	total[c]
SS	(0,0,1)	7A	−1.39	−0.93	−2.26	−4.58
surface	(1,1,1)	2A	0.00	−4.51	0.00	−4.51
DS	(0,0,1)	7B	−0.98	−1.84	−1.00	−3.82
TS	(1,1,1)	9A	−0.12	−2.76	−1.00	−3.88
QS	(1,1,1)	9B	+0.55	−3.68	−1.00	−4.13
QS	(0,0,1)	7C	+8.92	−3.68	?	+5.24

[a] CB:Ar$_n$ kernel clusters shown in Figures 8 and 9. V_{latt} is $I = 2$ option (cf. Table 4). [b] Special stabilization energies unique to each trapping site, see text. [c] The zero of energy is Ar$_n$ + CB. The CB surface site is modeled in Figure 2.

TABLE 6: Energy Shifts $\delta\Delta E_{site}$ (kcal/mol) and PES Minima Offsets Δ (cm^{-1}) for the Symmetry-Lowered SS Trapping Site[a]

	Ar atom displacements ($R_1 - r_0$) and ($R_2 - r_0$) (cf. Figure 4)							
	−0.05	+0.05	+0.00	+0.05	+0.00	+0.10	+0.05	+0.15
r_0, Å	$\delta\Delta E_{site}$	Δ	$\delta\Delta E_{site}$	Δ	$\delta\Delta E_{site}$	Δ	$\delta\Delta E_{site}$	Δ
3.97					−0.488	109	−0.855	88
4.07	−0.066	90	−0.189	27	−0.317	71	−0.472	56
4.17	−0.042	58			−0.122	45	−0.140	35

[a] Ar$_4$ moiety coplanar with CB in CB:Ar$_{12}$ kernel is offset to rectangular geometry; cf. R_1 and R_2 Figure 4.

slightly as pairs to bring the square Ar$_4$ configurations into rectangular conformations. The objectives were (a) to estimate the magnitude of the site relaxation energy from this source, and (b) to estimate the magnitude of the energy offset Δ arising between the energy minima of the two CB valence isomers in the (frozen) slightly asymmetric SS site.

Table 6 presents HI-MO energy differences computed over a grid of small displacements of the Ar$_4$ group to form rectangular geometry, while the basic geometry of the CB:Ar$_{12}$ clusters was determined by r_0 values of 3.97, 4.07, and 4.17 Å. The minimum for the $\Delta E_{site}^{(12,1)}$ curve is near 4.07 Å, as noted

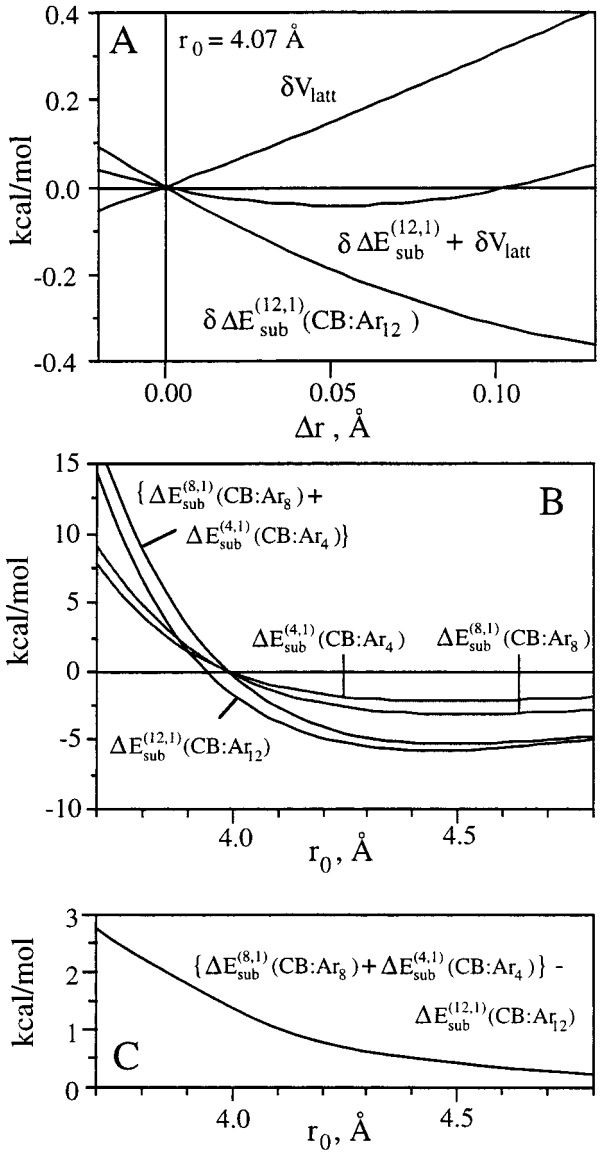

Figure 8. Energy for asymmetric distortion of $\Delta E_{site}^{(12,1)}$ with $r_0 = 4.07$ Å. (A) Plot of $\delta\Delta E_{site}^{(12,1)}$(CB:Ar$_{12}$) when the two Ar atoms on the axis paralleling the C−C bonds are dilated by Δr Å. δV_{latt} is expressed as (2/12)V_{latt}. (B) Comparison of $\Delta E_{sub}^{(12,1)}$(CB:Ar$_n$) curves, and demonstration that {$\Delta E_{sub}^{(4,1)}$(CB:Ar$_4$, planar) + $\Delta E_{sub}^{(n,1)}$(Ar$_4$:CB:Ar$_4$, stacked)} converges toward $\Delta E_{sub}^{(12,1)}$(CB:Ar$_{12}$). (C) Magnification of the convergent energy difference ΔE.

above. Table 6 shows that asymmetrically dilating the site based on $r_0 = 4.07$ Å to relax the C−C bonds with 0.05 and 0.10 Å Ar displacements lowers $\Delta E_{sub}^{(12,1)}$(CB:Ar$_{12}$) by −0.189 and by −0.317 kcal/mol, respectively. The Ar displacements correspond to increasing R_2 in Figure 4 and they are opposed by the V_{latt} PEF, which is appreciable in the r_0 range of 4.07 to 4.17 Å as seen in Figure 6D. Since only 2 of the 12 Ar atoms in the r_1 shell are given the asymmetrizing displacements, the opposing V_{latt} PEF is taken as (2/12)V_{latt} for the site. Table 3 then shows that the V_{latt} energy displacement, δV_{latt}, rises by 1.8528/6 = 309 cal/mol between $r_0 = 4.07$ and 4.17 Å. The opposing $\delta\Delta E_{sub}^{(12,1)}$(CB:Ar$_{12}$) and δV_{latt} functions are illustrated in Figure 8A, where it is seen that the offset of the two coplanar Ar atoms adds only tens of cal/mol to the stabilization energy of the SS site but demonstrates a soft PEF, suggesting fluxional behavior of the trapping site surroundings. This is important to the automerization dynamics of CB isolated in Ar. Table 6 also

shows the offset of the PES minima for the valence isomers is $\Delta = 27$ cm^{-1} and $\Delta = 71$ cm^{-1}, respectively, for 0.05 and 0.10 Å asymmetrizing displacements of the two Ar atoms. Table 1 showing $R_{C-C} - R_{C=C} = 0.220$ Å for gaseous CB suggests the two Ar atoms are likely to be displaced by an amount greater than 0.05 Å to produce ~50 cm^{-1} as a reasonable HI-MO value for Δ in the SS site.

The automerization mechanism of Ar-isolated CB is readily envisioned using the above HI-MO computed information. Assigned[11] at 723 cm^{-1}, the fundamental automerization vibration qualifies as a fast coordinate relative to the slow Ar lattice coordinates to suggest adiabatic separation of the vibrations. Since both CB and the trapping site configuration are nonrigid they develop equivalent minimum energy SS trapping site configurations, one for each valence isomer, in a process easily visualized by allowing CB:Ar$_4$ and its R_1 and R_2 coordinates in Figure 4 to symbolize the trapping site. With Ar/CB sojourning most of the time near one or the other of the PES minima, the fast automerization coordinate of CB usually faces an asymmetric double-minimum PES with $\Delta \sim 50$ cm^{-1}. Because the upper ZP level is thermally depopulated, no spectra are anticipated from this state and no transitions were observed experimentally. When the trapping site Ar atoms fluctuate to reach symmetrical site configurations to provide a transient equal double-minimum PEF for the CB automerization coordinate, the Ar/CB probability density function delocalizes and the CB valence isomers equally sample both of the nascent equivalent global PES minima. The experimental automerization rate of $\geq 10^3$ s^{-1} for Ar/CB provides a lower limit that is nearly 10^{-9} times the estimated automerization rate[11] for free CB. The spectroscopically identifiable vicinally dilabeled (^{13}C or D) valence isomers are found to have equal populations. This is an observation consistent with their equal occupancy of the two equivalent trapping sites made accessible by the fluxional nature of the SS trapping site environment.

Manz[21] considered a pseudorotation model for CO isolated in Ar wherein the distorted trapping site geometry rotates with CO. With automerization equivalent to a 90° rotation, the present situation is similar in its demand for a soft site PEF with modest values for the largest Ar displacements (e.g., 0.05−0.10 Å). As just shown, the properties computed for HI-MO Ar/CB are strongly supported by the unique dynamical/spectroscopic data produced by the research group of Michl.[2−4]

To conclude this section, it is of interest to consider the results of examining $\Delta E_{sub}^{(4,1)}$(CB:Ar$_4$, planar) and $\Delta E_{sub}^{(8,1)}$(Ar$_4$:CB:Ar$_4$, stacked), and adding them together to simulate $\Delta E_{sub}^{(12,1)}$(CB:Ar$_{12}$). The objective is to check the validity of using [V_{latt}/6] for δV_{latt} in the above asymmetric site analysis, and to determine the degree to which multibody interaction energies are lost at the interface joining the two small clusters. Figure 8B shows functions entering the equation

$$\Delta E = \Delta E_{sub}^{(12,1)}(\text{CB:Ar}_{12}) - [\Delta E_{sub}^{(4,1)}(\text{CB:Ar}_4, \text{planar}) + \Delta E_{sub}^{(8,1)}(\text{Ar}_4\text{:CB:Ar}_4, \text{stacked})] \quad (14)$$

It shows that $\Delta E_{sub}^{(4,1)}$(CB:Ar$_4$, planar) and $\Delta E_{sub}^{(8,1)}$(Ar$_4$:CB:Ar$_4$, stacked) are not drastically different in the $r_0 = 4.07$ to 4.17 Å range of interest to suggest that the (2/12) factor used with δV_{latt} is not unreasonable. The ΔE curve in Figure 8C is a measure of the magnitudes of multibody energy contributions deleted from consideration by summing the small cluster $\Delta E_{sub}^{(n,m)}$-(cluster) values to estimate $\Delta E_{sub}^{(12,1)}$(CB:Ar$_{12}$). For exclusively transferable two-body interactions with identical geometries for the Ar$_{12}$ moieties, this ΔE value would vanish exactly. For example, with X representing either CB or the central Ar atom in Ar$_{13}$, there are 32 pairwise Ar−Ar interactions in X:Ar$_{12}$ which are absent in enumerations of the pairwise Ar−Ar interactions in the isolated X:Ar$_4$ and Ar$_4$:X:Ar$_4$ clusters. The deleted 2-body terms are identical in the sums for the Ar:Ar$_{12}$ cluster and for the CB:Ar$_{12}$ cluster if the Ar$_{12}$ moieties in CB:Ar$_{12}$ and Ar:Ar$_{12}$ are identical, and they cancel along with a number of other terms in eq 14. Rather than vanishing, it is seen in Figure 8B for $r_0 = 3.77$ Å that the HI-MO ΔE value is −2.29 kcal/mol (i.e., 8.64 − 10.93 kcal/mol). In Figure 8C ΔE is seen to decrease steadily toward zero with increasing r_0.

3E. General Trapping Site Considerations. The discussion has concentrated on the single-substitutional trapping site and brought in surface adsorption energies, higher near-neighbor interaction energies, and the kernel-lattice interface. The considerations are now formalized for a CB:Ar$_N$ crystallite with N much larger than the modest n and m values chosen to describe a kernel cluster.

The isomerization reaction that converts an Ar crystallite with an adsorbed CB into a defect crystallite hosting internally trapped CB is written

$$\text{CB}^{ads}\text{:Ar}_N \rightarrow \text{CB:Ar}_{N-m}^{displ}\text{:}m\text{Ar}^{ads} \quad (15)$$

The superscript "ads" indicates the adsorption of CB or of Ar onto an outer surface of the fcc crystallite, and the superscript "displ" indicates Ar atoms near the defect site are displaced from their ideal lattice positions. The site energy defined by the reaction in eq 15 is written

$$\Delta E_{site}^{(N-m,m)} = \Delta E_f(\text{CB:Ar}_{N-m}^{displ}\text{:}m\text{Ar}^{ads}) - \Delta E_f(\text{CB}^{ads}\text{:Ar}_N) \quad (16)$$

and the $\Delta E_{site}^{(N-m,m)}$ value can, in principle, be evaluated by adding a series of thermochemical equations such as those following, where the energy symbols are given their anticipated algebraic signs.

Desorption of CB from the crystallite surface

$$\text{CB}^{ads}\text{:Ar}_N \rightarrow \text{CB} + \text{Ar}_N \qquad +\Delta E_{CB}^{ads} \quad (17)$$

Extraction of an Ar_{n+m} kernel from the crystallite interior

$$\text{Ar}_N \rightarrow \text{Ar}_{N-n-m} + \text{Ar}_{n+m} \qquad +\Delta E_{kern(Ar)} \quad (18)$$

Substitution of CB into an m-Ar vacancy of the Ar_n kernel

$$\text{Ar}_{n+m} + \text{CB} \rightarrow \text{CB:Ar}_n^{displ} + m\text{Ar} \qquad \pm\Delta E_{sub}^{(n,m)}(\text{CB:Ar}_n) \quad (19)$$

Deformation of the Ar crystallite lattice atoms surrounding the kernel site vacancy to accommodate the CB:Ar_n^{displ} kernel

$$\text{Ar}_{N-n-m} \rightarrow \text{Ar}_{N-n-m}^{displ} \qquad \pm V_{latt} \quad (20)$$

Insertion of the CB:Ar_n^{displ} kernel into the prepared vacancy in the crystallite

$$\text{Ar}_{N-n-m}^{displ} + \text{CB:Ar}_n^{displ} \rightarrow \text{CB:Ar}_{N-m}^{displ} \qquad -\Delta E_{kern(CB:Ar)} \quad (21)$$

Adsorption of the m Ar atoms onto the crystallite surface

$$\text{CB:Ar}_{N-m}^{displ} + m\text{Ar} \rightarrow \text{CB:Ar}_{N-m}^{displ}\text{:}m\text{Ar}^{ads} \qquad -\text{m}\Delta E_{Ar}^{ads} \quad (22)$$

The surface desorption and adsorption steps, eqs 17 and 22, have energies of opposite sign and could conceivably cancel, but HI-MO computations on the Ar/CB system suggest they must be kept. It is noted that the zero of energy in Table 5 is taken as Ar_N + CB rather than as CB adsorbed onto the cluster as in eq 15.

Equations 18 and 21 reflect the oppositely signed energies for extraction of a neat Ar_{n+m} cluster and its replacement by the CB:Ar_n^{displ} kernel cluster. For a sufficiently large n value, these two terms would cancel because the V_{latt} (eq 20) energy would become negligible and the kernel-vacancy interfaces arising for reactions 18 and 21 would match undistorted fcc crystal surfaces. Equations 19 and 20 are the r_0-dependent energies appearing in Figure 6 and are used to generate a first approximation for properties of the SS site.

3D. Double-, Triple-, and Quadruple-Ar Substitutional Sites in Ar/CB. Figure 7 illustrates the kernel clusters used to investigate double-, triple-, and quadruple-substitutional sites with CB lying in the (0,0,1) plane of fcc Ar. Figure 7A shows the CB:Ar_{12} kernel cluster used for the single-substitutional vacancy with the Ar_{12} moiety given dark shading. Figures 7B and 7C show the CB:Ar_{18} and CB:Ar_{26} kernel clusters used for the DS and QS vacancies. Triple-substitutional sites with CB lying in the (0,0,1) plane were not investigated in detail, but the basic geometrical considerations are clear in Figure 7. Figures 9A and 9B show the CB:Ar_{15} and CB:Ar_{16} kernels used for the triple- and quadruple-substitutional vacancies with CB lying in the (1,1,1) plane of fcc Ar. In the computations, however, these kernels were given hcp (ABAB...) stacking. At the r_0 values of most interest, test computations showed differences of less than 10 cal/mol between the fcc and hcp stackings. Figure 7 shows that in CB:Ar_{12} the CB molecule makes close vdW contacts with 12 Ar atoms, while in CB:Ar_{18} and CB:Ar_{26} there are 8 and 2 close CB−Ar contacts, respectively. All of the kernel clusters in Figures 7 and 9 make close Ar-π system contacts (cf. Figure 3), and for some the Ar-π PES topography determines the CB orientation in the vacancy.

The double-substitutional vacancy hosting CB in a (0,0,1) plane (Figure 7B) relaxes the snug SS site and could conceivably achieve the greater stability. The D_{2h} CB:Ar_{18} configuration in Figure 7B has lower energy than configurations with CB shifted to one side. With r_0 = 3.97, 3.17, and 4.37 Å the D_{2h} $\Delta E_{sub}^{(18,2)}$(CB:Ar_{18}) energies are −2.353, −1.469, and −0.924 kcal/mol relative to the SS-like C_{2v} configuration, although in the lattice the stabilization at the 3.77 Å point would be reduced to −2.353 − (−1.13) = −1.22 kcal/mol due to interaction of CB with the two non-kernel second nn Ar atoms in the manner described for the SS site.

With r_0 = 4.17 Å, the HI-MO energy difference between the CB valence isomers in the D_{2h} CB:Ar_{18} kernel cluster is very large at Δ = 6.60 kcal/mol. This result is due to interaction between the stacked Ar atoms and the π system of CB as demonstrated by separate HI-MO $\Delta E_{sub}^{(n,2)}$(CB:Ar_n) computations on the planar CB:Ar_6 and the stacked Ar_6:CB:Ar_6 clusters. At r_0 = 4.17 Å the Δ values are 0.568 and 6.044 kcal/mol, respectively, for these clusters to demonstrate near additivity of the small-cluster Δ values to the Δ = 6.60 kcal/mol value. Figure 7B shows that the pairs of Ar atoms in low energy positions above and below the CB plane acquire repulsive Ar-π interactions when CB automerizes in frozen Ar_{18} geometry.

Rotation of CB about the long axis of the DS vacancy brings it into the (1,1,1) plane of the CB:Ar_{18} kernel cluster. This configuration can be imagined from Figure 2 by replacing the two central Ar atoms in Ar_{10} with CB oriented with its C−C bonds paralleling the long axis, and with 5 Ar atoms added as an fcc stacked upper layer. This configuration of CB:Ar_{18} is destabilized because its narrow waist in the (1,1,1) plane brings the coplanar Ar atoms between the H atoms of the (HC)−(CH) linkages. At r_0 = 3.77 Å, $\Delta E_{sub}^{(10,2)}$(CB:Ar_{10}, (0,0,1)) = +6.241 kcal/mol versus $\Delta E_{sub}^{(8,2)}$(CB:Ar_8, (1,1,1)) = +21.021 kcal/mol. For r_0 = 4.17 Å, $\Delta E_{sub}^{(10,2)}$(CB:Ar_{10}) = −0.278 kcal/mol and, while $\Delta E_{sub}^{(8,2)}$(CB:Ar_8) would also be lowered as r_0 increases, it would remain above $\Delta E_{sub}^{(10,2)}$(CB:Ar_{10}). The strong stabilization of the stacked (0,0,1) cluster seen for the DS site would also favor CB lying in the (0,0,1) plane. HI-MO energies for the DS site energetics are shown in Table 7. V_{latt} is adapted to the DS vacancy by estimating that 8, rather than 12, Ar atoms in the kernel-lattice interface layer qualify as first nearest-neighbors, while ignoring other changes. The leading 12 in the r_1 shell of V_{latt} (eq 11) is thus changed to 8(7/12) = 4.667.

The stabilization energy contribution of $\Delta E_{site}^{(18,2)}$ = $\Delta E_{sub}^{(18,2)}$(CB:Ar_{18}) + V_{latt} to the DS site is only −0.98 kcal/mol, and this is entered into Table 5 along with −1.84 kcal/mol due to surface adsorption of 2 Ar atoms. For the DS site stabilization energy to equal that of the SS site would require more than −2

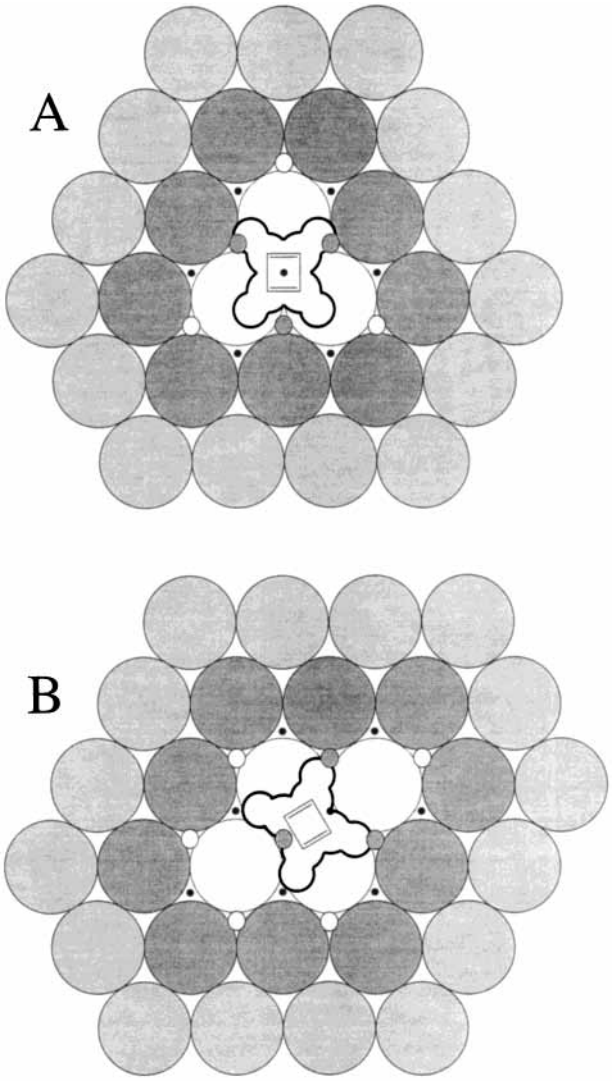

Figure 9. Definitions for CB:Ar_n kernel clusters and m-Ar vacancies with CB lying in the (1,1,1) plane of fcc Ar. (A) TS site, CB:Ar_{15} kernel. (B) QS site, CB:Ar_{16} kernel. Together with CB the darker shaded Ar atoms indicate the (hcp) CB:Ar_n kernel clusters. The small circles and heavy dots represent Ar atoms in the planes above and below the plane of CB.

TABLE 7: HI-MO Energies for Double-Substitutional Site in Ar/CB (CB in (0,0,1) Plane)[a]

r_0	ΔE_f(Ar:Ar$_{20}$)	ΔE_f(CB:Ar$_{18}$)	$\Delta E_{sub}^{(18,2)}$	V_{latt}[b]	$\Delta E_{sub}^{(18,2)c}$	Δ
3.37	9.9905			27.0846		
3.57	−8.1170			7.4585		
3.77	−13.7808			0.7149		
3.97	−14.1879	−15.6019	−1.4140	0.4388	−0.9752	
4.17	−12.6545	−16.5845	−3.9300	3.5943	−0.3357	6.600
4.37	−10.6180	−15.1964	−4.5784	8.3015	3.7231	
4.57	−8.6426			13.8913		
4.77	−6.9161			16.3202		

[a] CB:Ar$_{18}$ kernel cluster in Figure 7B. ΔE energy definitions in eqs 3, 4, 6, and 13. r_0 is Å and energies are kcal/mol. [b] Equation 9. Lead "12" in eq 11 is adapted to 8(7/12) = 4.6667; see text. [c] Stabilization energy contribution: −0.98 kcal/mol at r_0 = 3.97 Å.

TABLE 8: HI-MO Energies for Triple-Substitutional Site in Ar/CB (CB in (1,1,1) Plane)[a]

r_0	ΔE_f(Ar:Ar$_{18}$)	ΔE_f(CB:Ar$_{15}$)	$\Delta E_{sub}^{(15,3)}$	V_{latt}[b]	$\Delta E_{site}^{(15,3)c}$	Δ
3.57				8.1604		
3.77	−10.3688	−8.8359	1.5332	0.7769	2.3101	1.001
3.97	−10.7587	−11.2361	−0.4774	0.3605	−0.1169	0.406
4.17	−9.6277	−10.9021	−1.2744	3.0077	1.7333	0.145
4.37	−8.0934	−9.5795	−1.4861	7.0604	5.5743	0.038

[a] CB:Ar$_{15}$ kernel cluster in Figure 9A. ΔE energy definitions in eqs 3, 4, 6, and 13. r_0 is in Å and energies are kcal/mol. [b] Equation 9. Lead "12" in eq 11 is adapted to 9(7/12); see text. [c] Stabilization energy contribution: −0.12 kcal/mol at r_0 = 3.97 Å.

kcal/mol from a source that is unique to the DS site, e.g., an outward displacement of Ar atoms at its waist. The scale of the available displacement energies is indicated by the Δ value for the coplanar CB:Ar$_{10}$ cluster, 0.568 kcal/mol at r_0 = 4.17 Å, and −1 kcal/mol is entered as a reasonable top value $\Delta E_{sub}^{(n,m)}$(cluster) into column 6 of Table 5.

The CB molecule fits snugly into the triangular triple-subsitutional vacancy in the (1,1,1) plane of the unrelaxed HI-MO Ar lattice with r_o = 3.88 Å, as seen in Figure 9A. The relevant energetics are listed in Table 8, where a stabilization of −0.12 kcal/mol is obtained from $\Delta E_{site}^{(15,3)}$. This is entered into Table 5 along with −2.76 kcal/mol for the surface adsorption of three Ar atoms. Figure 9A suggests translation of CB toward the base of the site and/or outward displacement of the two coplanar Ar atoms impinged by CH bonds as possible sources of special site stabilization. For r_0 = 4.17 Å with CB on the symmetry axis of hcp stacked Ar$_3$:CB:Ar$_3$ the Δ value is only 0.005 kcal/mol, while for planar CB:Ar$_9$ the Δ value is 0.156 kcal/mol. The sum is a few percent over the Δ = 0.145 kcal/mol value of CB:Ar$_{15}$. Trial HI-MO computations with r_0 = 3.77 Å yield relaxation energies in the −1 or −2 kcal/mol range for displacements of the above types, but at r_0 values ≥ 3.97 Å the relaxation energies are much smaller and −1 kcal/mol is again offered for site-specific stabilization energies as entered into Table 5. The triple vacancy with CB in the (0,0,1) plane was not investigated in detail but it is also expected to be less stable than the SS site. As discussed for the QS (1,1,1) kernel cluster, the PES of the TS site has a vivid topography when the rotational axes for CB and Ar$_3$:CB:Ar$_3$ do not coincide.

The 4-Ar vacancy shown in Figure 9B for the (1,1,1) plane is larger than CB and interesting in terms of CB rotational orientation. If CB is rotated about 45° from its illustrated position, four of the coplanar Ar atoms nearly match Ar positions in the CB:Ar$_4$ vdW configuration (cf. Figure 4). With fcc stacking CB is centered in the CB:Ar$_{16}$ kernel cluster at all rotational angles, and it was kept centered when rotated for computations in the hcp stacked clusters. The planar CB:Ar$_{10}$ and hcp stacked Ar$_3$:CB:Ar$_3$ clusters were separately examined to isolate the π cloud and coplanar Ar effects on the angular orientation of CB. In the planar cluster with r_0 = 3.77 Å, the conformation with CB rotated by 45° is stabilized by −0.550 kcal/mol over the 0° and 90° conformations (where Δ is only 34 cal/mol). As suggested by the data in Table 8, this orientational energy would be reduced for r_0 = 3.97 Å.

TABLE 9: HI-MO Energies for Quadruple-Substitutional Site in Ar/CB (CB in (1,1,1) Plane)[a]

r_0	ΔE_f(Ar:Ar$_{20}$)	ΔE_f(CB:Ar$_{16}$)	$\Delta E_{sub}^{(16,4)}$	V_{latt}[b]	$\Delta E_{site}^{(16,4)c}$	Δ
3.57			6.0547			
3.77	−11.3902	−10.9026	0.4876	0.5911	1.0787	
3.97	−11.8518	−11.5821	0.2697	0.2822	0.5519	1.781
4.17	−10.6217	−10.4928	0.1289	2.4211	2.5500	1.103
4.37	−8.9373	−8.9178	0.0195	5.8193	5.8388	

[a] CB:Ar$_{16}$ kernel cluster in Figure 9B. ΔE definitions in eqs 3, 4, 6, and 13. r_0 is Å and energies are kcal/mol. [b] Equation 9. Lead "12" in eq 11 is adapted to 6(7/12); see text. [c] Stabilization energy contribution: +0.55 kcal/mol at r_0 = 3.97 Å.

TABLE 10: HI-MO Energies for Quadruple-Substitutional Site in Ar/CB (CB in (0,0,1) Plane)[a]

r_0	ΔE_f(Ar:Ar$_{30}$)	ΔE_f(CB:Ar$_{26}$)	$\Delta E_{sub}^{(26,4)}$	V_{latt}[b]	$\Delta E_{site}^{(26,4)c}$	Δ
3.57				3.8488		
3.77				0.3964		
3.97	−24.2616	−12.9450	11.3166	0.2001	11.5167	0
4.17	−21.4903	−14.3790	7.1113	1.8066	8.9179	0
4.37				4.5191		

[a] CB:Ar$_{26}$ kernel cluster in Figure 7C. ΔE energy definitions in eqs 3, 4, 6, and 13. r_0 is Å and energies are kcal/mol. [b] Equation 9. Lead "12" in eq 11 adapted to 2(7/12); see text. [c] Destabilized trapping site.

In the QS vacancy the rotational axis for CB does not coincide with the Ar$_3$:CB:Ar$_3$ symmetry axis, and this brings into play the strong geometry dependence of the Ar-π cloud interactions. When r_0 is 4.17 Å, rotating the CB molecule in 15° steps provides the relative orientational energies 0.000, 0.4746, and 1.0943 kcal/mol at rotational angles of 0° (Figure 9B), 45°, and 90°. At r_0 = 3.97 Å these values are 0.000, 0.6864, and 1.7759 kcal/mol, and at r_0 = 3.77 Å they are 0.000, 0.9393, and 2.865 kcal/mol. The combined coplanar and stacked orientational energies show that CB:Ar$_{16}$ has the configuration of Figure 9B with a relatively soft CB librational PEF near the minimum. With Δ = 1.781 kcal/mol at r_0 = 3.97 Å for the CB:Ar$_{16}$ kernel cluster (Table 9), the above data reiterate the near additivity of Δ values computed for the planar and stacked moieties to the full cluster Δ value. Allowing −1 kcal/mol for relaxation energies that are unique to the QS site, e.g., contraction of Ar atoms coplanar with CB to reduce the free volume of the vacancy, again leaves it less stable than the SS site as seen in Table 5.

The QS vacancy with CB lying in the (0,0,1) plane (Figure 7C) was examined using a CB:Ar$_{26}$ kernel cluster as shown in Table 10. The $\Delta E_{site}^{(26,4)}$ value of this centrosymmetric configuration is very high, +8.92 kcal/mol, probably due to the absence of close CB−Ar interactions. This QS site might gain stabilization energy through a shift of CB to offset positions resembling those of the DS or SS sites.

4. Summary and Concluding Remarks

The HI-MO (MP2/6-311++G(2d,2p) trapping site stability ranking for Ar/CB appears in Table 5. The single-substitutional site is the most stable by a small margin, evidently due to strongly stabilizing interactions arising through the nearly congruent shapes of the C_4H_4 molecule and the SS vacancy in

the (0,0,1) plane of the fcc Ar crystal lattice. The stabilization energy for the SS site is estimated as a very reasonable −4.6 kcal/mol. Increasing the level of MO theory and, even more importantly, enlarging the kernel cluster to CB:Ar_{18} or larger to include the n_2 lattice shell would increase the reliability of the estimate for SS trapping site stabilization, in good part by incorporating directly into the kernel cluster computation several interaction energies that had to be separately estimated in the present work.

Small displacements of the four nearest-neighbor Ar atoms coplanar with CB are made to induce rectangular distortion of the SS site. There is very little additional stabilization energy, but a soft PEF is demonstrated for displacements of this type in HI-MO Ar/CB. This is an important result because, with CB surrounded by a soft layer of boundary Ar atoms, the SS site can readily distort to provide two equivalent, exchangeable, PES minima for occupancy by the CB valence isomers. Between extended sojourns with small site fluctuations localizing the Ar/CB system to one or the other of the PES minima, there are larger fluctuations bringing the site to symmetrical configurations intermediate between the two global PES minima. For symmetrical site configurations the fast CB automerization coordinate vibrates in a nominal equal double-minimum PEF to delocalize the site probability density function. In this state the Ar/CB system can readily shift between the two equivalent PES minima. The situation is symbolized in Figure 4, where the important R_1 and R_2 coordinates are emphasized.

The HI-MO automerization model readily explains the available matrix-isolation experimental data[2−4] for Ar/CB. ^{13}C-NMR and IR polarization measurements on cold Ne/CB or Ar/CB matrix samples with vicinally dilabeled $^{13}C_2$−CB show that the automerization occurs at rate $\geq 10^3$ sec^{-1} in the matrix. This lower limit provides room for the soft SS site fluctuations to decrease the fast estimated free molecule automerization rate[11] by a factor as small as 10^{-9} in Ar/CB, where site exchange must accompany the valence isomerization. There are no apparent spectroscopic tunneling doublets in the observed vibrational spectra[2−4] of matrix-isolated CB despite the prediction[11] of a zero-point tunneling splitting of about 11 cm^{-1} for free CB. Analysis of the Raman experiment[10] led to the conclusion that in the Ar matrix the ZP levels are separated by $\Delta \geq 35$ cm^{-1} as an experimental observation, and $\Delta \sim 50$ cm^{-1} is estimated from the HI-MO computations for slightly asymmetric SS site configurations. Vibration of the fast automerization coordinate normally takes place in the asymmetric SS site environment, where it is subjected to an unequal double-minimum PEF. With $\Delta \sim 50$ cm^{-1}, the upper ZP level is thermally depopulated and transitions from this state are absent in the spectra. When slightly larger fluctuations in the right direction bring the SS site to symmetrical configurations the fast CB automerization coordinate vibrates in a nominally equal DM PEF to delocalize the probability density function of the site and to foment exchange of the system between the equivalent global PES minima. The exchange certainly occurs because equal populations of the two vicinally dilabeled and therefore clearly identifiable matrix-isolated (^{13}C or D) valence isomers are indicated by their IR/Raman transitions. Equal populations of the valence isomers are compatible with a large Δ value and site asymmetry only when the trapping site geometry fluctuates to provide regularly exchanged equivalent PES minima for the distinguishable valence isomers. In a near-rigid asymmetric trapping site only one valence isomer, the one most stabilized by the asymmetric site, would generate spectra in the low-temperature experiments.

Analysis of the oscillating probability density function for a 1-D asymmetric double-minimum PEF using the approach presented by Hameka and de la Vega[22] convincingly shows that, for an asymmetric DM PEF with a Δ offset of 75 cm^{-1} and a barrier maximum of 1750 cm^{-1}, an appreciable probability density persists in the high-energy well. In a cold temperature bath the upper ZP level is depopulated but readily accessible, and with an appropriate site fluctuation the Ar/CB system can shift from one equivalent global PES minimum to the other.

Substitutional sites based on *m*-Ar vacancies are not only HI-MO computed to be less stable than the SS site, but they do not provide an experimentally required low-barrier route between equivalent global PES minima. Figures 7 and 9 show that in *m*-Ar sites the valence isomers are locked into a specific PES well of the site. The HI-MO Δ values are usually large and, with large intrasite PES barriers to be passed, extreme fluxional behavior of the lattice (or of the guest) would be required for the Ar/CB system to transfer between equivalent PES minima of the sites.

Dilation of the nearest-neighbor Ar shell of the HI-MO SS site is estimated as 0.19 Å, and this value is consistent with the 0.3−0.4 Å dilations computationally derived[19,20] for Ar/FCH_3 and for Ar/FH_2CCH_2F. The HI-MO stabilization energy of −4.8 kcal/mol for the SS site in Ar/CB is a reasonable value that depends on the V_{latt} function used to approximate the radial distortion energy of the fcc lattice about the CB guest molecule. This function is independent of any data fitting procedure; however, the version utilized in the computations was subjectively chosen. It is the function most intermediate in character between the V_{latt} limits of zero damping and full damping of the dilation volume ΔV in the lattice shells beyond r_1. This subjective decision is seen to provide highly objective results. There are obvious reasons to expect that HI-MO computations on a system as complex as Ar/CB would lack quantitative accuracy. The work presented here, however, provides sufficiently comprehensive qualitative and semiquantitative conclusions that the basics of the automerization mechanism become transparent. The mechanism is seen to be in excellent agreement with carefully prepared and unique spectroscopic measurements[2−4] reported for the Ar/CB system.

Acknowledgment. The author is grateful to the Robert A. Welch Foundation for support of this research.

References and Notes

(1) Carpenter, B. K. *J. Am. Chem. Soc.* **1983**, *105*, 1700.
(2) Orendt, A. M.; Arnold, B. R.; Radziszewski, J. G.; Facelli, J. C.; Malsch, K. D.; Strub, H., Grant, D. M.; Michl, J. *J. Am. Chem. Soc.* **1991**, *110*, 2648.
(3) Arnold, B. R.; Michl, J. *J. Phys. Chem.* **1993**, *97*, 13348.
(4) Arnold, B. R.; Radziszewski, J. G.; Campion, A.; Perry, S. S.; Michl, J. *J. Am. Chem. Soc.* **1991**, *113*, 692.
(5) Balkova, A.; Bartlett, R. J. *J. Chem. Phys.* **1994**, *101*, 8972.
(6) Carsky, P.; Bartlett, R. J.; Fitzgerald, G.; Noga, J.; Spirko, V. *J. Chem. Phys.* **1988**, *89*, 3008.
(7) Nakamura, K.; Osamura, Y.; Iwata, S. *Chem. Phys.* **1989**, *136*, 67.
(8) Carsky, P.; Spirko, V.; Hess, B. A., Jr.; Schaad, L. J. *J. Chem. Phys.* **1990**, *92*, 6069.
(9) Carsky, P.; Downing, J. W.; Michl, J. *Int. J. Quantum Chem.* **1991**, *40*, 415.
(10) Carsky, P.; Michl, J. *Theor. Chim. Acta* **1992**, *84*, 125.
(11) Redington, R. L. *J. Chem. Phys.* **1998**, *109*, 10781.
(12) Ha, T.-K.; Pochert, J.; Quack, M. *J. Phys. Chem. A* **1998**, *102*, 5241.
(13) Hollenstein, D.; Luckhaus, D.; Pochert, J.; Quack, M.; Seyfang, G. *Angew. Chem. Int. Ed. Engl* **1997**, *36*, 140.
(14) Frisch, M. J.; Trucks, G. W.; Schlegel, H. B.; Gill, P. M. W.; Johnson, B. G.; Robb, M. A.; Cheeseman, J. R.; Keith, T.; Petersson, G. A.; Montgomery, J. A.; Raghavachari, K.; Al-Laham, M. A.; Zakrzewski, V. G.; Ortiz, J. V.; Foresman, J. B.; Cioslowski, J.; Stefanov, B. B.;

Nanayakkara, A.; Challacombe, M.; Peng, C. Y.; Ayala, P. Y.; Chen, W.; Wong, M. W.; Andres, J. L.; Replogle, E. S.; Gomperts, R.; Martin, R. L.; Fox, D. J.; Binkley, J. S.; Defrees, D. J.; Baker, J.; Stewart, J. P.; Head-Gordon, M.; Gonzalez, C.; Pople, J. A. *Gaussian 94*, revision A.1; Gaussian, Inc.: Pittsburgh, PA, 1995.

(15) Aziz, R. A. *J. Chem. Phys.* **1993**, *99*, 4518.

(16) Lotrich, V. F.; Szalewicz, K. *J. Chem. Phys.* **1997**, *106*, 9688.

(17) Redington, R. L., manuscript in preparation.

(18) Bemish, R. J.; Block, P. A.; Pedersen, L. G.; Yang, W.; Miller, R. E. *J. Chem. Phys.* **1993**, *99*, 8585.

(19) (a) Gunde, R.; Felder, P.; Gunthard, H. H. *Chem. Phys.* **1982**, *64*, 313. (b) Gunde, R.; Gunthard, H. H. *Chem. Phys.* **1987**, *111*, 339. (c) Gunde, R.; Keller, H. J.; Ha, T.-K.; Gunthard, H. H. *J. Phys. Chem.* **1991**, *95*, 2802.

(20) Lakhlifi, A.; Girardet, C. *J. Chem. Phys.* **1989**, *90*, 1345.

(21) Manz, J. *J. Am. Chem. Soc.* **1980**, *102*, 1801.

(22) Hameka, H. F.; de la Vega, J. R. *J. Am. Chem. Soc*. **1984**, *106*, 7703.